

# Numerical and Experimental Investigations of Simple 2-D Geometries in Slamming

Adrian Constantinescu<sup>1</sup>, Aboulghit El Malki Alaoui<sup>2</sup>, Alain Neme<sup>2</sup> and Philippe Rigo<sup>1</sup>

## ABSTRACT

*The paper presents a numerical and experimental study of slamming phenomena experienced by rapid ships during the impact of its bow on the water surface. The numerical research work covers the finite element modeling of the impact between a rigid body and a free water surface. Three numerical approaches were tested. Firstly, a semi-FEM tool based on the finite element code ABAQUS/Standard is performed in order to calculate pressures, energies and global forces during slamming. The second analysis represents fully FE simulations of slamming with ABAQUS/Explicit. The modeling uses a viscous, compressible and irrotational fluid and a soft-exponential fluid-solid contact law. The third numerical approach is based on the newest multiphysics capability Coupled Eulerian-Lagrangian (CEL) of ABAQUS developed under FE ABAQUS/Explicit v6.7. Experimental slamming tests achieved with the new shock experimental facility at the ENSIETA laboratory validated these numerical approaches.*

## KEY WORDS

Slamming; Fluid-structure interaction; ABAQUS/Explicit; Coupled Eulerian-Lagrangian (CEL); Shock machine.

## INTRODUCTION

In 1929 Von Karman (1929) took note about slamming experiments carried out on seaplane floats in the U.S.A. and developed an analytical formulation to obtain the maximal pressure trained on these floats during the sea landing. Two years later, Wagner (1932) formulates a more realistic model by taking into account the elevation of the free water surface, parameter neglected by Von Karman.

Initially studied for seaplane floats, the slamming phenomena quickly began important in the naval field. This dynamic, random and non-linear impact induces local and global harmful effects. Concerning the global responses, the whole ship is brutally subjected to a bending moment and a shearing force, introducing general vibrations of the beam hull ship. The local response describes more especially the local damages due to repeated impacts on the exterior hull. These responses affect also the crew and passengers comfort and the integrity of embarked equipments. In these conditions, it is important to predict exactly the applied forces for a correct and optimal design.

According to Bertram (2002), the wave impact caused by the slamming can be roughly classified into four types: bottom, 'bow-flare', breaking wave and wet-deck. The paper treats only the bottom slamming, i.e. impact between the inferior hull structure and the free water surface. Even if the slamming is a fully three-dimensional phenomenon, we limit our study to simple rigid geometries (2D and pseudo-3D) and 2D flows, as a first step to develop numerical methods for deformable and 3D cases. Slamming forces depend on the deadrise angle between body and free water surface. With air trapping the mechanism of impact becomes more complex. The effects generated by the presence of air cannot be neglected for deadrise angles lower than 4° (Langrand 2001). Our study is then limited to deadrise angles between 4° and 45° according to Wagner theory.

---

<sup>1</sup> University of Liege, ANAST, Liege, Belgium

<sup>2</sup> ENSIETA, LBMS - EA 4325 - ENSIETA / Université de Brest / ENIB, Brest, France

## ABAQUS/STANDARD APPROACH (IMPACT++)

### Analytical formulation

We consider the impact problem of a body on a water surface, according to the [Figure 1](#). The fluid problem is formulated within potential flow theory for an ideal fluid (incompressible, inviscid, irrotational), initially at rest. We assume small disturbances for the fluid and the solid domain, and we neglect the gravity. The flow is analyzed using eulerian variables and must fulfill the conservation of mass and the momentum equation.

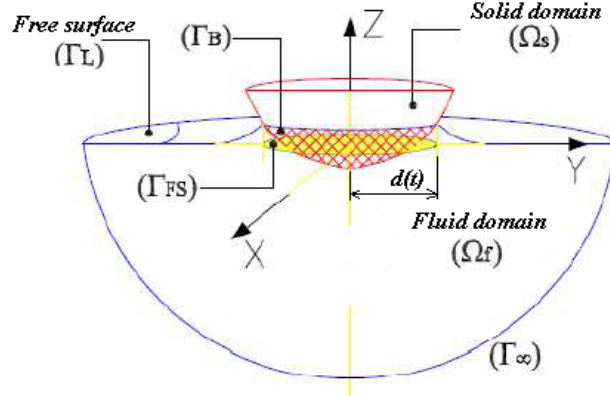


Figure 1: Geometric definition

The velocity vector anywhere in the fluid domain is obtained as  $V_f = \mathbf{grad} \Phi$  and the velocity potential  $\Phi(x, y, z, t)$  must satisfy the continuity, sliding, free surface condition and decay conditions, Equations 1 to 4.

$$\Delta \Phi = 0 \quad \text{in the fluid domain } \Omega_f \quad [1]$$

$$\mathbf{grad} \Phi \cdot \mathbf{n} = V_s \cdot \mathbf{n} \quad \text{on the wetted surface } \Gamma_B, \text{ where } V_s \text{ is the impact speed of the solid} \quad [2]$$

$$\Phi = 0 \quad \text{on the free surface } \Gamma_L \quad [3]$$

$$\mathbf{grad} \Phi = 0 \quad \text{far from the body } \sqrt{(x^2 + y^2 + z^2)} \rightarrow \infty \quad [4]$$

Keeping the non-linear limit conditions, the fluid problem is very complex. To simplify the fluid formulation, previous limit conditions will be projected on the initial water surface ( $z = 0$ ). The free surface is a material surface. Its elevation  $h$ , relative to its initial position, allows us to write a second boundary condition for the free surface, Equation 5. The non-stationary version of the Bernoulli equation establishes the formula for the hydrodynamic pressure, Equation 6. In Equation 6, the second term represents the steady state dynamic pressure. The values of the pressure are non-null only on the surface in contact with the body, named wet surface.

$$\frac{\partial \Phi}{\partial z} = \frac{\partial h}{\partial t} \quad \text{on the free surface, where } h = \int_0^t \frac{\partial \Phi}{\partial z} \Big|_{(x,y,0,\tau)} d\tau \quad [5]$$

$$p = -\rho_f \frac{\partial \Phi}{\partial t} - \frac{1}{2} \rho_f (\mathbf{grad} \Phi)^2 \quad [6]$$

The extend of the wet surface, denoted  $d(t)$  in Figure 1, represents the intersection between the free surface rising and the position of the solid body. The integral in time of the normal derivative of the velocity potential expresses the free surface elevation. Thus, we can solve the problem of the displacement potential  $\Psi = \Psi(x, y, z, t)$  such that:

$$\Psi = \int_0^t \Phi(x, y, z, t) dt \quad \text{and} \quad h = \frac{\partial \Psi}{\partial z} \Big|_{(x,y,0,t)} \quad [7]$$

The completely hydrodynamic fluid problem requires thus two calculations. The first uses the displacement potential to obtain the real wet surface and the second calculates the hydrodynamic pressure on the wetted surface using the velocity potential. In case of the displacement potential  $\Psi$ , the limit conditions are similar with those of the velocity potential, Equations 1 to 4, with the remark that only the vertical components of  $\Psi$  are relevant.

## Numerical modeling

### Fluid – head transfer analogy

The numerical model uses the fluid-head transfer analogy to solve the fluid dynamics problem. Donguy (2002) developed a numerical approach to simulate the slamming problems using this approach under the FE code CASTEM. We have globally followed the same approach using the industrial FE code ABAQUS associated with PYTHON and FORTRAN languages instead of CASTEM. Our developed code was generically named Impact++ ABAQUS after Impact++ CASTEM.

Under the hypotheses of incompressibility and irrotational initial velocity field for the fluid, the temperature  $T$  expresses the velocity potential  $\Phi$  and the displacement potential  $\Psi$ . The heat transfer model is given by the following equations:

$$\Delta T = 0 \quad \text{in the fluid domain } \Omega_f \quad [8]$$

$$\lambda \frac{\partial T}{\partial z} = -\mathbf{q} \cdot \mathbf{z} \quad \text{on the wetted surface } \Gamma_{FS} \quad [9]$$

$$T = 0 \quad \text{on the free surface } \Gamma_L \quad [10]$$

$$\frac{\partial T}{\partial z} = \frac{\partial h}{\partial t} \quad \text{on the free surface } \Gamma_L \quad [11]$$

In Equation 9,  $\mathbf{z}$  stands for the unit vertical vector. If the temperature  $T$  is expressed in  $[\text{m}^2/\text{s}]$ , the thermal conductivity is set to  $\lambda = 1$ , and  $\mathbf{q} = -\mathbf{v} = -\mathbf{grad} \Phi$  is expressed in  $[\text{m}/\text{s}]$  in the head module of ABAQUS/Standard, the above system express the velocity potential problem being similar to system given by Equations 1 to 5. For the displacement potential, we use the same system, Equations 8 to 11, but the temperature  $T$  will be consequently expressed in  $[\text{m}^2]$  with thermal conductivity  $\lambda = 1$  and  $\mathbf{q}$  in  $[\text{m}]$ .

### Mesh and FE calculations particularities

For a complete analysis of slamming, the total time of analysis is decomposed into major increments of time  $\Delta t$ . The numerical evaluation of the hydrodynamic pressure, Equation 6, requires at each time increment  $\Delta t$ , two calculations of the velocity potential. A smaller time increment  $\delta t$  is used in order to obtain two velocity potentials at  $t_j (= j \Delta t)$  and  $t_j + \delta t$  respectively. In rigid case and only for structures having constant deadrise angles, the value of  $\Delta t$  establishes the frequency of output database. This time increment is also very important for a correct simulation of the fluid-structure coupling in the deformable case. The  $\Delta t$  increment is also an important parameter for a good estimation of  $\dot{d}(t)$  by central differencing, Equation 12. The distances  $d(t_i)$  and  $d(t_{i-1})$  are the wet surface distances calculated respectively at two consecutives increments  $t_i$  and  $t_{i-1}$  ( $t_i - t_{i-1} = \Delta t$ ).

$$\dot{d}(t) = \frac{d(t_i) - d(t_{i-1})}{\Delta t} \quad [12]$$

The value of  $\delta t$  depends on the smallest mesh size  $M_s$  around the contact surface border and on the wet surface velocity  $\dot{d}(t)$ . The value of  $\delta t$  must be greater than  $M_s / \dot{d}(t)$  to compute accurately the contact surface dimension, but it must be also small enough to determine correctly the pressure field. Finally, a value of  $\Delta t/3$  was retained for  $\delta t$ .

To obtain accurate values of the wet surface distances at every time increments, we employ numerical iterations with a convergence criterion, contrary to Impact++ CASTEM approach which uses an approximate Wagner model. The convergence criterion is:

$$d_k - d_{k-1} \leq \text{aprox. } 2M_s \quad [13]$$

To take into account the high potential gradient, the extremity of the wet surface was meshed with a very fine grid, Figure 2. In this zone, the smallest mesh size  $M_s$  should be lower than the dimension of the physical singularity. The jet thickness  $\delta_{jet}$  can be a good approximation of this dimension. Nevertheless, the smallest mesh size is determined by the accuracy of  $\dot{d}(t)$  which strongly influences the quality of the pressure peak evaluation. We can estimate the logarithmic

error of  $\dot{d}(t)$  as  $\frac{\Delta \dot{d}(t)}{\dot{d}(t)} = \frac{M_s}{d(t) \delta t}$ . In case of wedges  $\dot{d}(t) = \frac{\pi}{2} \frac{V}{\tan \beta}$  and we can prove that the  $M_s$  is given by the Equation 14.

$$M_s = \frac{\pi}{2} \frac{V}{\tan \beta} \delta t \frac{\Delta \dot{d}(t)}{\dot{d}(t)} \quad [14]$$

Choosing  $\frac{\Delta \dot{d}(t)}{\dot{d}(t)} \leq 10^{-2}$ , for the least restrictive case ( $V = 20$  m/s and  $\beta = 6^\circ$ ) we find  $M_s \leq 2 \mu\text{m}$ , and for the most restrictive case ( $V = 1$  m/s and  $\beta = 14^\circ$ ) we find  $M_s \leq 0,4 \mu\text{m}$ . We finally chose the smallest mesh size  $M_s$  between  $1 \mu\text{m}$  and  $2 \mu\text{m}$  in order to verify the convergence criterion while keeping a reasonable CPU time.

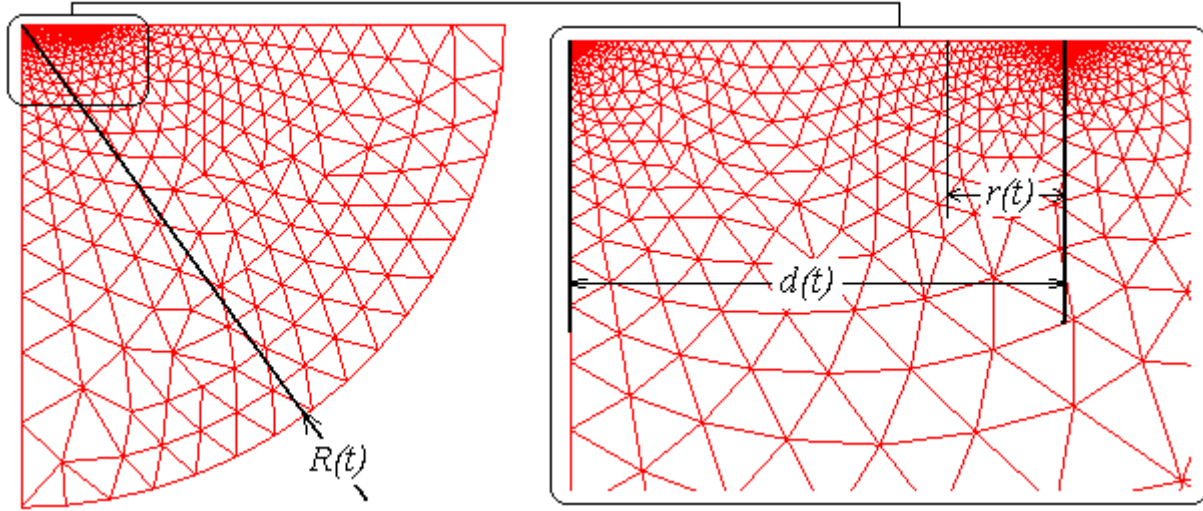


**Figure 2: Fluid mesh**

We optimized the fluid mesh reducing the number of elements successively while checking the convergence of the results. We found numerically that, during the analysis, the minimal number of elements is approximately between 3000 (at the beginning, first increment) and 5700 (at the end, last increment). The dimension of the meshed fluid zone is dynamically adapted to the contact surface between solid and water  $R(t) = 8d(t)$ , [Figure 2](#). For a smaller value of  $R(t)$ , the total effort is overestimated especially at the onset of impact.

The FE calculations for the displacement potential  $\Psi$  employ this type of mesh to compute accurate wet surfaces at each increment of time  $\Delta t$ . The input data in the displacement potential calculus are the positions of the body into the water. The input data in velocity potential  $\Phi$  calculations are the length of the wet surface and the speed impact of the body into the water. To obtain the velocity potentials we adopted a special technique, valid only for constant entry speed cases and for a given shape form of the rigid body at time. The main idea is to realize a single calculus of the velocity potential  $\Phi$  and the **grad**  $\Phi$  considering a reference impact speed of 1 m/s and a reference wet surface of 1 m. This “non-dimensional” calculus will provide the reference velocity potential  $\Phi_r(y, z)$  and the reference gradient **grad**  $\Phi_r(y, z)$ . These values are fixed for a given shape form of the body. Returning to an Impact++ ABAQUS simulation, after each displacement potential calculus, on the new wet surface  $d(t)$ , the real potential  $\Phi(y, z = 0)$  and the real gradient **grad**  $\Phi$  are obtained using Equation 15 and Equation 16 respectively.

$$\Phi(y, 0) = V \cdot \Phi_r\left(\frac{y}{d(t)}, 0\right) \cdot d(t) \quad [15]$$

$$\text{grad} \Phi(y, 0) = V \cdot \text{grad} \Phi_r\left(\frac{y}{d(t)}, 0\right) \quad [16]$$

where  $V$  represents the speed impact of the rigid body. We remark that the velocity potential calculations are independently of deadrise angle  $\beta$ . Using the technique described above, the CPU time is reduced up to 40% compared to the case where the velocity potential  $\Phi$  was obtained by a FE calculation at each time increment.

Mis  
Gras  
Supp

### Pressure particularities

The calculation of the final pressure is associated with an asymptotic development at the wetted surface boundary. The asymptotic study led to the determination of two zones (inner and far-field) in which two asymptotic developments are obtained. The far-field solution (fulfilling conditions far from the body-surface intersection, but being singular at the intersection, Equation 17) and the near-field solution (valid near to the intersection, describing the formation of a jet, Equation 18) have to be connected for the correct evaluation of the resulting total force.

$$p_{far} = -\rho_f \frac{\Phi_{t+\delta t} - \Phi_t}{\delta t} - \rho_f \frac{(\mathbf{grad}\Phi_t)^2}{2} \quad [17]$$

$$p_{near} = \rho_f \frac{\dot{d}(t)^2}{2} \left( 1 - \left( \frac{1-u}{1+u} \right)^2 \right) \quad [18]$$

where  $u$  is determined by the resolution of the below non-linear system, Equation 19.

$$\begin{cases} y - d(t) = \frac{\delta_{jet}}{\pi} \left( 2 \ln u - \frac{4}{u} - \frac{1}{u^2} + 5 \right), & \text{for } y \leq d(t) \\ y - d(t) = \frac{\delta_{jet}}{\pi} \left( -2 \ln u - 4u - u^2 + 5 \right), & \text{for } d(t) < y \leq d(t + \delta t) \end{cases} \quad [19]$$

In the above equation, the parameter  $\delta_{jet}$  stands for the jet thickness. Due to divergent flow in axisymmetric configuration, the jet thickness is greater for dihedron case compared to cone case. Equation 20 gives the jet thickness in 2D case. According to Scolan's (2001) investigations, Equation 21 provides the same parameter in axisymmetric case.

$$\delta_{jet}^{dihedron} = \frac{\pi V^2 d(t)}{8 \dot{d}(t)^2} \quad [20]$$

$$\delta_{jet}^{cone} = \frac{1}{2\pi} \frac{V^2 d(t)}{\dot{d}(t)^2} \quad [21]$$

Taking into account analytical formula for wet surface  $d(t)$  and wet surface velocity  $\dot{d}(t)$ , a simple calculus shows that the jet thickness is double for dihedron compared to cone, for identical impact speed and deadrise angle, as presented in the [Table 1](#).

**Table 1: Analytical formula for dihedron and cone**

Case	$d(t)$	$\dot{d}(t)$	$\delta_{jet}$
Dihedron (2D)	$\frac{\pi}{2} \frac{V t}{\tan \beta}$	$\frac{\pi}{2} \frac{V}{\tan \beta}$	$\frac{1}{4} V t \tan \beta$
Cone (pseudo 3D)	$\frac{4}{\pi} \frac{V t}{\tan \beta}$	$\frac{4}{\pi} \frac{V}{\tan \beta}$	$\frac{1}{8} V t \tan \beta$

Since we used numerical resolution and finite distances from the exact wetted surface boundary, an approximate model is necessary to connect analytical far-field and near-field pressure solutions. The operating range of this connection is limited to the distance  $r(t) = V t$  in front of the end of wet surface, as in Figure 2, where  $V$  is the constant plunging velocity. The connection between far-field and near-field pressures is achieved through the link pressure  $p_{link}$ , Equations 22 and 23, and the corrected link pressure  $p_{link}^c$ , Equations 24:

$$p_{link} = \rho_f \frac{V d(t) \dot{d}(t)}{\sqrt{2d(t)(d(t) - y)}} \quad \text{for dihedron} \quad [22]$$

$$p_{link} = \rho_f \frac{V d(t) \dot{d}(t)}{\pi \sqrt{d(t) \frac{(d(t) - y)}{2}}} \quad \text{for cone} \quad [23]$$

$$\begin{cases} p_{link}^c = p_{link}, & \text{for } y \leq d(t) - r \\ p_{link}^c = p_{far} + \left( \frac{d(t) - y}{r} \right)^2 [p_{link} - p_{far}], & \text{for } d(t) - r < y \leq d(t) \end{cases} \quad [24]$$

To avoid singular values of  $\mathbf{grad}\Phi(y, z)$  at  $(y, z) = (d(t), 0)$ , we use  $\mathbf{grad}\Phi(y, z)$  at  $(y_0, z_0) = (d(t) - r, 0)$  to evaluate  $p_{far}$ , from Equation 17, in Equation 24 whatever  $y$  between  $d(t) - r$  and  $d(t)$ . The second order term of the Equation 24 ensures the non-influence of the corrected link pressure into the form of the near-field pressure. The final pressure is given by the sum of the far-field and near-field pressures and subtracting their common part, Equation 25.

$$p_{num}^f = p_{far} + p_{near} - p_{link}^c \quad [25]$$

From these previous set of equations, we can find the maximal pressure  $p_{max}$  given by the near pressure, Equation 26.

$$p_{max} = p_{near}|_{u=1} = \rho_f \frac{\dot{d}(t)^2}{2} \quad [26]$$

## ABAQUS/EXPLICIT APPROACH

### Fluid Equation of State

The second numerical approach is based on the capabilities of commercial finite element software ABAQUS/Explicit to simulate unsteady fluid flows using Arbitrary Lagrangian-Eulerian (ALE) analysis. This adaptive meshing technique combines the feature of pure Lagrangian analysis and pure Eulerian analysis. According to the ABAQUS documentation (HKS 2004), flow modeling of compressible fluid can be achieved by using the linear  $U_s-U_p$  form of the Mie-Grüneisen equation of state. This equation, particularly useful at high pressure, defines the pressure as function of the density  $\rho$  and of the internal energy per unit mass  $E_m$  of the fluid, Equation 27.

$$p = f(\rho, E_m) \quad [27]$$

The equation for conservation of energy equates the increase in internal energy per unit mass,  $E_m$  to the rate at which work is being done by the stresses and the rate at which heat is being added. In the absence of heat conduction, Equation 28 gives the energy equation.

$$\rho \dot{E}_m = p \frac{1}{\rho} \dot{\rho} + tr(S \dot{\epsilon}_d) + \rho \dot{Q} \quad [28]$$

where  $p$  is the pressure,  $S$  is the deviatoric stress tensor,  $\dot{\epsilon}_d$  is the deviatoric part of strain rate, and  $\dot{Q}$  is the heat rate per unit mass. By eliminating the internal energy from Equations 27 and 28, under negligible shear stresses and lack of any heat source assumptions, we obtain the Mie-Grüneisen equation of state, Equation 29.

$$p - p_H = \Gamma \rho (E_m - E_H) \quad [29]$$

$$\Gamma = \Gamma_0 \frac{\rho_0}{\rho} \quad [30]$$

where  $p_H = f(\rho)$  is the Hugoniot pressure,  $E_H = f(\rho)$  is specific Hugoniot energy,  $\Gamma$  is the Grüneisen ratio given by Equation 30.  $\Gamma_0$  is a material constant and  $\rho_0$  is the reference density. The linear  $U_s-U_p$  Hugoniot form provides the Hugoniot pressure given by the Equation 31 where  $\eta$  is the nominal volumetric strain  $\eta = 1 - \rho_0/\rho$ .

$$p_H = \frac{\rho_0 c_s^2 \eta}{(1 - s\eta)^2} \quad [31]$$

The terms  $c_s$  and  $s$  define the linear relationship between the linear shock velocity  $U_s$  and the particle velocity  $U_p$ , Equation 32. The term  $c_s$  corresponds to the sound velocity at small nominal strains.

$$U_s = c_s + sU_p \quad [32]$$

With the above assumptions, the Equation 33 gives the pressure in the fluid.

$$p = \frac{\rho_0 c_s^2 \eta}{(1-s\eta)^2} \left( 1 - \frac{\Gamma_0 \eta}{2} \right) + \Gamma_0 \rho_0 E_m \quad [33]$$

The classical Newtonian fluid model defines the deviatoric response of the fluid, Equation 34. In below equation,  $\sigma_D$  is the deviatoric stress,  $\hat{D}_D$  is the deviatoric rate-of-deformation tensor and  $\mu$  is the viscosity of the fluid respectively.

$$\sigma_D = 2\mu \hat{D}_D \quad [34]$$

The equation of state can be used with all solid continuous elements (excepting elements working in plan strain case). Thus, we model the fluid with solid elements that have properties of fluid. In our simulations, the equation of state is defined by the parameters presented in [Table 2](#).

**Table 2: Equation of state parameters – ABAQUS/Explicit ALE**

$c_0$ [m.s <sup>-1</sup> ]	$s$ [-]	$\Gamma_0$ [-]	$\mu$ [-]	$\rho_0$ [kg.m <sup>-3</sup> ]
1425	1.75	0.28	0.001	1000

## Finite element modeling

As in Impact++ ABAQUS simulations, the fluid domain must be greater than the solid dimensions in order to avoid the numerical errors and not overestimate fluid pressures. In the present approach, the fluid is compressible. Waves in compressible media travel at finite speed. Therefore, the pressure acting on the structure will not depend on the size of the fluid domain if the non-return of shock waves condition, Equation 35, is satisfied. In this relation,  $L$  is the minimal distance between the structure and the limits of the fluid domain at maximum draught and  $T$  is the time of the simulation.

$$L \geq \frac{c_0 T}{2} \quad [35]$$

To minimize the CPU time, only in the superior part of the fluid, near to the structure, the mesh uses 4-node quadrilateral elements with bilinear interpolation functions and reduced integration (CPE4R in the plane strain problems and CAX4R for axisymmetric problems). In order to prevent severe mesh distortion, the very fine fluid mesh (element size about 150  $\mu\text{m}$ ) is associated with the adaptive meshing technique. The inferior part of the fluid, in which the deformation of the fluid remains moderate, is modeled with a Lagrangian mesh using triangular linear elements (CPE3 or CAX3). The [Figure 3](#) shows the partial fluid mesh.

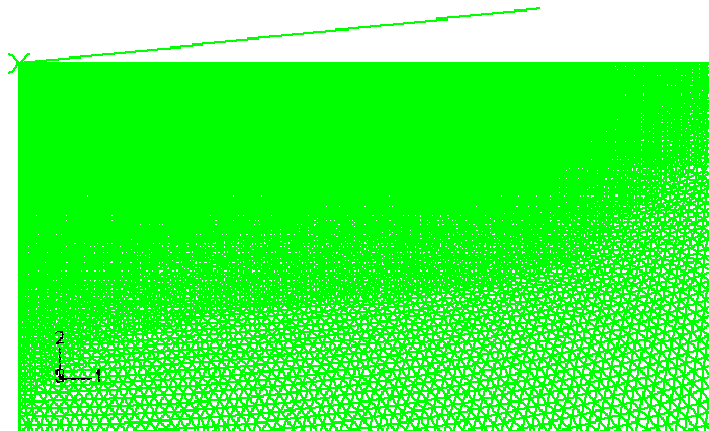


**Figure 3: Fluid mesh near to the structure - ABAQUS/Explicit**

Having only one integration point, the CPE4R and CAX4R elements may suffer from hourglassing. It is possible for them to distort in such a way that the strains calculated at the integration point are zero, which, in turn, leads to uncontrolled distortion of the mesh. In order to prevent this phenomenon, the elements include an hourglass control type

“Combined” which associates a stiffness and viscous term, Equation 36.

$$Q = \frac{1}{2} \left( K q + C \frac{dq}{dt} \right) \quad [36]$$

The term  $q$  is an hourglass mode,  $Q$  is the force (or moment) conjugated to  $q$ , and  $K$  and  $C$  are stiffness and viscous coefficients. The stiffness term acts to maintain a nominal resistance to hourglassing throughout the simulation, whereas the viscous term generates additional resistance to hourglassing under dynamic loading conditions.

To model the interaction between the structure and the fluid, we adopt a frictionless contact type. In the ABAQUS software, several methods are available for modeling the contact interface behavior. By default, a “hard” contact pressure-overclosure relationship is proposed for both surface-based contact and element-based contact. This type of contact do not allows penetration between surface (impenetrability condition) and conducts in our case to high oscillations of the peak pressure. In our simulations, we have used the “softened” pressure-overclosure relationship, which leads to a regularization of the impenetrability condition. The pressure-overclosure relation is prescribed by using an exponential law, presented in [Figure 4](#).

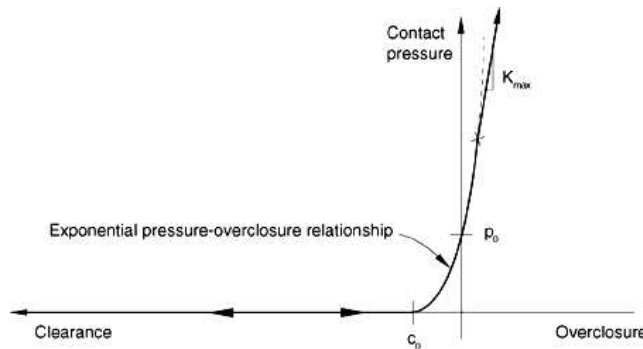


Figure 4: Exponential “softened” contact

This law depends on two principal parameters:  $c_0$  and  $p_0$ . The surfaces begin to transmit contact pressure once the clearance between them, measured in the contact (normal) direction, reduces to  $c_0$ . The contact pressure transmitted between the surfaces then increases exponentially as the clearance continues to diminish. These two parameters should be carefully selected such that interpenetrations between the fluid and solid surfaces remain small. Constantinescu (2006) performed a parametric study to understand the effect of these parameters. He observed that it is possible to obtain smooth solutions using very small interpenetrations between the surfaces (of the order of 10  $\mu\text{m}$ ). By combining these parameters with those presented in [Table 2](#), we obtain good results concerning the movement of fluid, [Figure 5](#), and [Figure 6](#), but also for spatial and temporal pressure, and effort distribution in rigid case for wedges and cones comparing with results issued from Impact++ ABAQUS and FLUENT codes. The results are presented later in this paper.

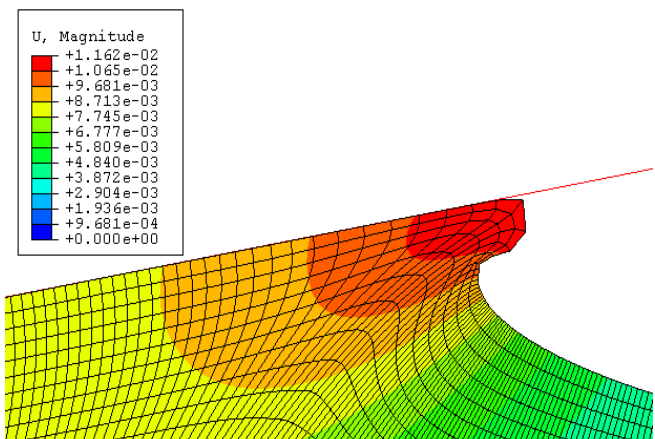


Figure 5: Fluid movement with ABAQUS/Explicit

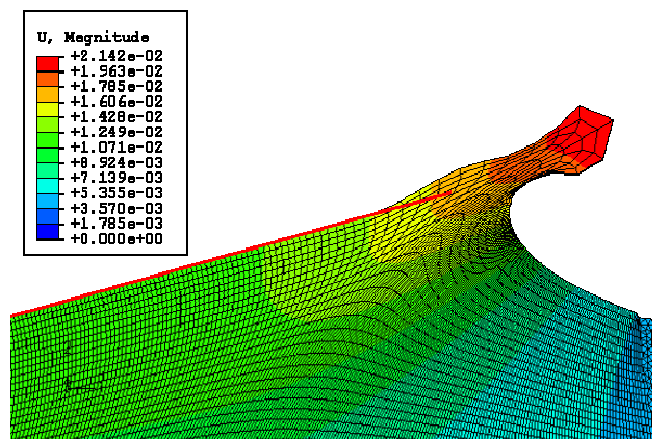


Figure 6: Structure entirely immersed

This approach has some advantages over the Impact++ approach. Thus, the modeling is not restricted to moderate deadrise angles. More important, it allows to deals with 3D problems. The slamming phenomena in deformable case can be directly treat within Abaqus, without rely on the coupling of other software product for the structure.

## COUPLED EULERIAN - LAGRANGIAN (CEL) APPROACH

The pure Eulerian analysis capability in Abaqus/Explicit allows for effective modeling of applications involving extreme deformation, including fluid flow. The Eulerian capability can be coupled with traditional Lagrangian capabilities to model interactions between highly deformable materials and relatively stiff bodies, such as in fluid-structure interactions. The principle of calculation is based on the Volume of Fluid method (VOF). The method is based on a fraction function, commonly denoted  $C$ . It is defined as the integral of fluid's characteristic function in the control volume, namely volume of a computational grid cell. Thus, inside each cell of the eulerian mesh, the scalar variable  $C$  increases gradually as the fluid moves into the cell. Basically, when the cell is empty (there's no traced fluid inside) value of  $C$  is zero, if cell is full, we have  $C = 1$ .

This recent possibility offered by ABAQUS remains for the moment limited to 3D models and eulerian field meshed using brick elements. For this reason we could not benefit completely from the axisymetry of the problem of which we modeled the quarter, as showed in [Figure 7](#). The quarter of cone is represented by a non-deformable rigid body. The volume of water is represented by a cube having an edge length of 0.8 m. The superior zone of the mesh (thickness of 0.05 m) is represented by vacuum zone. The fluid and vacuum zones constitutes the eulerian domain. The mesh grid remains very perfectible, but it allows obtaining suitable hydrodynamic efforts using approximately 190000 elements. According to [Figure 8](#), the finest grid is localized near to the interaction zone between the cone and water. Inside this cubic zone (edge length 0.2 m), the dimension of the mesh elements is around 5 mm.

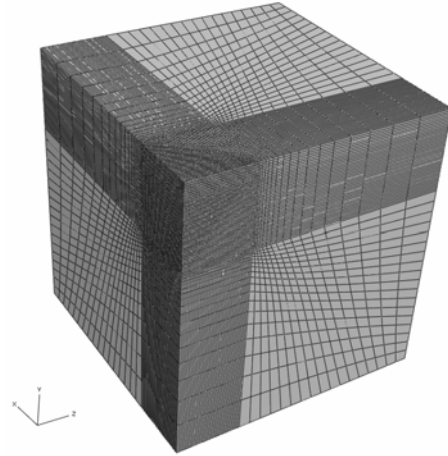
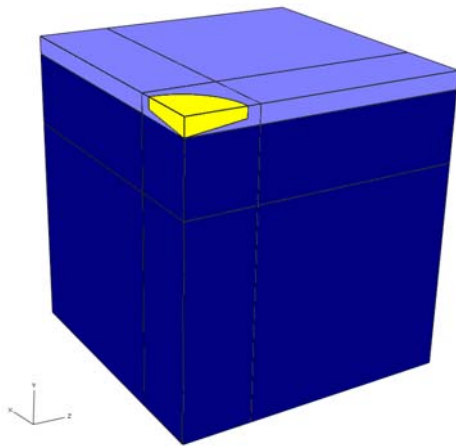


**Figure 7: Fluid, vacuum and cone domains**      **Figure 8: Fluid, vacuum and cone meshes**

ABAQUS/Explicit CEL uses the same equation of state as ABAQUS/Explicit ALE, equation already presented in the previous section. Only its parameters are slightly different.

**Table 3: Equation of state parameters – ABAQUS/Explicit CEL**

$c_0$ [m.s <sup>-1</sup> ]	$s$ [-]	$\Gamma_0$ [-]	$\mu$ [-]	$\rho_0$ [kg.m <sup>-3</sup> ]
1414	0	0	0.001	1000

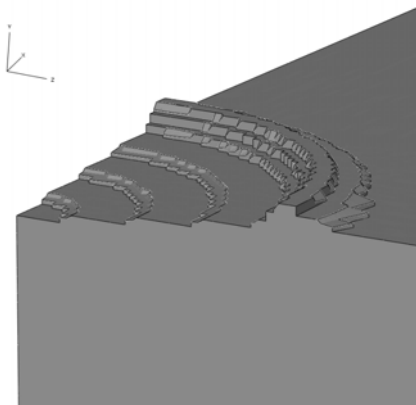


**Figure 9: Fluid deformation 3 ms after impact Cone, deadrise angle 7°, impact velocity 8 m/s**

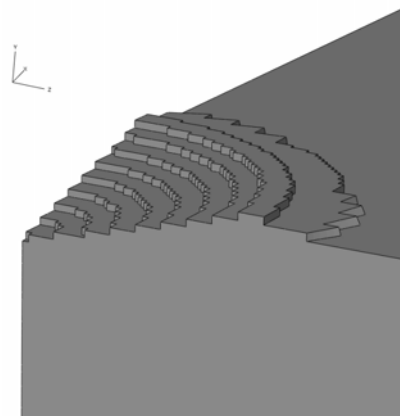


**Figure 10: Fluid deformation 3 ms after impact cone, deadrise angle 15°, impact velocity 15 m/s**

Mis e  
Gras  
Supp  
Supp  
Mis e  
Gras

The contact between the cone and water is modeled using frictionless hard contact model. Excepting the two inside surfaces of the fluid domain and the free face of the empty field, the three exterior faces of the eularian field are regarded as “stick” walls where the three components material speeds are null. The lower quality of the grid mesh does not allow to represent the formation of the jet. However, we observe the formation of waves and we correctly verify the axisymmetry of the problem, according to the [Figure 9](#), and [Figure 10](#).

## EXPERIMENTAL INVESTIGATIONS

### Experimental set-up

At ENSIETA laboratory, we carried out experimental tests in order to obtain experimental data to validate the previous numerical approaches. The investigation consists of impact tests with simple structures using a hydraulic shock machine, presented in [Figure 11](#). This machine is rather unique according to its performances and its flexibility for the reason that crushing test on solids can be also conducted. Its numerical control with internal model allows controlling the displacement and the impact velocity of the plunger piston.



Figure 11: Shock machine and its water tank



Figure 12: Experimental setup of the rigid cone

We have tested two types of cones (seven and fifteen degrees). The structure is fixed at the extremity of the plunger piston through an intermediate support, as presented in [Figure 12](#). The fluid tank is mounted under the shock device and is filled with 1.1 m height of fresh water.

The design of the structures (cones) must respect certain conditions. The structure is made in massive aluminum alloy to assure minor inertial forces and very small overall deformation. In case of cones, the deadrise angle  $\beta$  must allow an easier visualization of the free water surface. The impact force should be high enough in order to guarantee a satisfactory signal/noise ratio, but must not overstep the shock machine limits. For each type of structure, several Impact++ ABAQUS simulations allowed to calculate the maximal force and thus to obtain the optimal impact velocity.

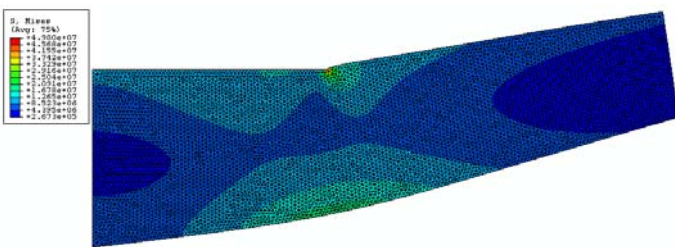


Figure 13: Cone under flexion with magnification ratio

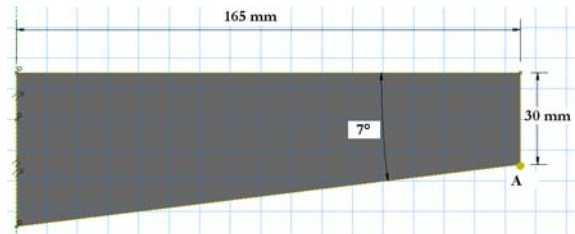


Figure 14: Positioning of the point A which corresponds to maximum displacement under flexion (case of cone  $\beta = 7^\circ$ )

The flow experiment in semi-infinite medium is ensured by the ratio between dimensions of the tank and those of the structures. In order to avoid boundary effects, the maximum diameter of these parts must be lower than  $1/6^{\text{th}}$  of the smaller characteristic length of the basin (i.e. the width). The diameter and deadrise angle being fixed, the height of parts was determined with respect to a stiffness criterion. This criterion corresponds to a deflection of the structure’s end (noted A on [Figure 14](#)) smaller than  $50 \mu\text{m}$ , which corresponds to the manufacture tolerance.

The geometries were numerically tested with ABAQUS/Standard in order to obtain this maximal deflection, [Figure 13](#). The [Figure 14](#) presents the final dimensions of the aluminum alloy cone having a  $\beta = 7^\circ$  deadrise angle.

For the two rigid cones characterized by deadrise angles  $\beta = 7^\circ$  and  $\beta = 15^\circ$ , the use of the Equation 38 combined with the Wagner's linearized theory made it possible to plot an estimate of maximum hydrodynamic effort according to the impact speed. These curves, presented in [Figure 15](#), allow identifying the "ideal" points of functioning for the tests relatively to machine capability, namely:

- $V_{\max} = 10$  m/s for  $\beta = 7^\circ$  with a maximal force  $F \approx 99.4$  kN;
- $V_{\max} = 16$  m/s for  $\beta = 15^\circ$  with a maximal force  $F \approx 98.0$  kN.

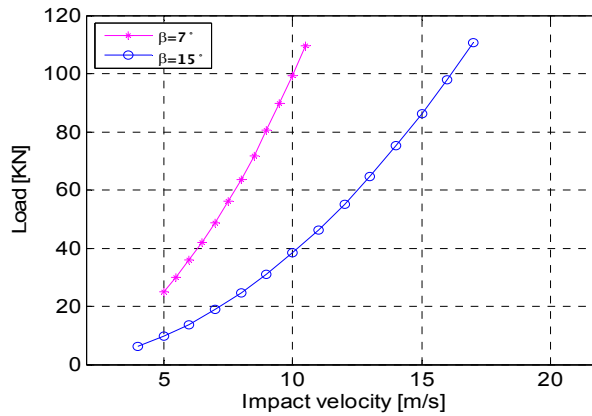


**Figure 15: Force – speed diagram for cones ( $\beta = 7^\circ$  and  $\beta = 15^\circ$ )**

[Table 4](#), presents the various impact velocities employed for each type of cone. In order to ensure the results reproducibility, each test has been repeated at least three times.

**Table 4: Values of impact velocity employed for each cone**

Deadrise angle $\beta$	$7^\circ$			$15^\circ$		
Impact velocities [m/s]	5.0	6.5	8.0	8.0	12.0	15.0

## Experimental instrumentation

During the impact tests, displacement, acceleration and force measurements are performed. An internal machine sensor measures the piston displacement at 2.5 kHz sampling frequency. A piezoresistive sensor type EGAS-FS-\* -250-/V12/L8M/X, placed on the cone, measures the acceleration, [Figure 16](#). It has an effective range of  $\pm 250$  g, a sensitivity of 0.32 mV/g, an eigen frequency of 2.5 kHz, a damping coefficient of 0,64 and a voltage supply of 12 V. The acceleration measurements allow us to quantify the inertial forces due to slightly non-constant velocity during the impact. Four FFG-2-1K-C1-11 KYOWA™ gauges located at 50 mm from the piston extremity measure the impact force, [Figure 16](#). The KYOWA gauges are connected in Wheatstone full bridge to a NICOLET™ data acquisition system recording at a sampling rate of 20 kHz. The electrical signal delivered by the acceleration sensor is recorded on the same data acquisition system at the same sampling frequency.

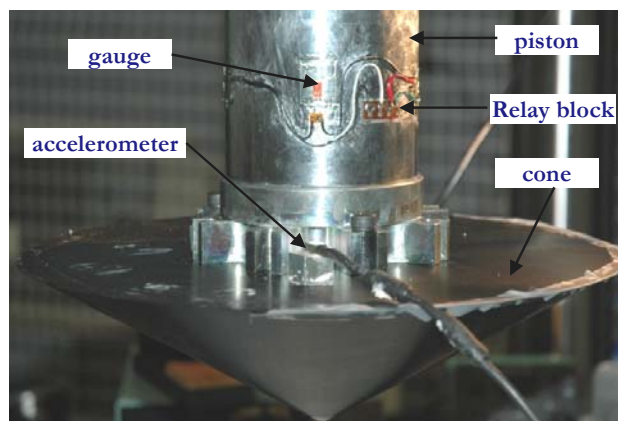


**Figure 16: Accelerometer implantation and gauges positioning**

We have also used an electrical detection system to identify correctly the real time contact between the cone and water. In fact, this time represents the start of the numerical simulations. The NICOLET™ data acquisition system records the voltage in an electrical circuit that changes its impedance when the cone touches the water.

In addition to basic acquisition systems (force, displacement, acceleration), we also used a PHOTRON high speed digital video camera to record the evolution of the interaction between cone and water in a window of 1024x128 pixels at 15000 frames per second. For this purpose, the camera is placed near to a circular window of the lateral side of the basin, [Figure 11](#). These circular windows, having a diameter of 0.7 m, are made in PMMA (PolyMethyl MethAcrylate). The [Figure 17](#), shows several photos of this fluid-structure interaction.

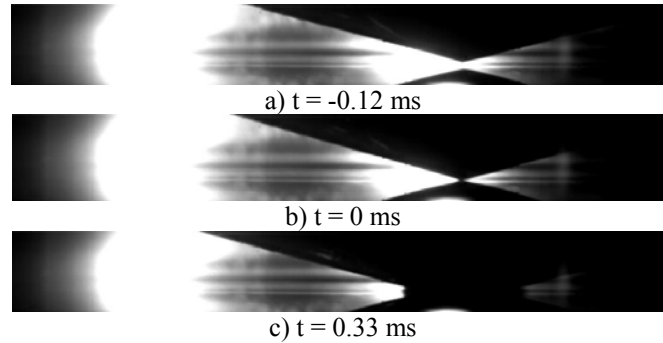


**Figure 17: Photos obtained during the impact of a 15° deadrise angle cone at 15 m/s**

The force gauges were already calibrated in order to establish a relation between the force  $F$  and the variation of relative voltage variation  $\Delta u/U$  at the terminals of the Wheatstone bridge. The speed and the displacement are calculated successively by a simple and double numerical integration of the acceleration signal. An optimization procedure of the displacement and a temporal retiming made it possible to calibrate the accelerometer and to obtain the inertial efforts. The results show, on one hand, that the stabilized impact speed is not strictly constant and, on the second hand, that resultant accelerations are more disadvantageous as the mass of the structure is important.

## RESULTS COMPARISON

### Comparisons between numerical approaches

Initially, we compared the results obtained using Impact++ ABAQUS with those of Impact++ CASTEM. The main differences between the two codes refer to calculus of the wet surface extend  $d(t)$  and to calculus of the inner pressure for cones. Donguy (2002) used an analytical estimation, whereas we employ an iterative process with convergence criterion. In case of cones, Donguy don't correct the inner pressure and the analytical correction formula, and applied the equations used for the wedge case. However, in our simulations the maximum pressure values agree very well with those determined with CASTEM (Constantinescu 2006). We also obtain the same wet surface propagation velocity, as well as the resulting vertical force on the solid.

The first comparisons between Impact++ ABAQUS and ABAQUS/Explicit reveal satisfactory results concerning spatial and temporal pressures, and effort distribution. As shown in [Figure 18](#), with ABAQUS/Explicit the pressure peaks evolution of spatial distributions is well reproduced regarding the Impact++ results. Initially, the ABAQUS/Explicit response has an oscillatory due to initial contact between solid and fluid that repose on a small number of elements mesh, and then it stabilizes.

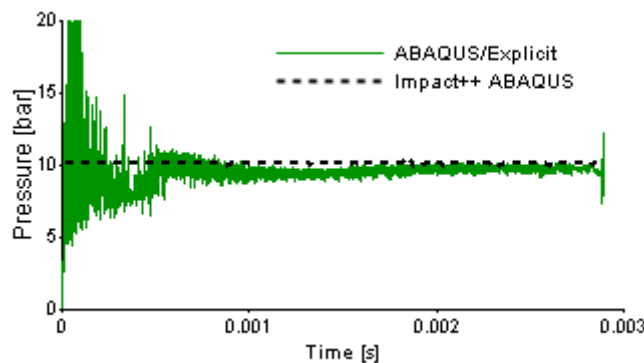


**Figure 18: Peaks pressure evolution for a rigid wedge  $\beta = 10^\circ$ ,  $V = 5$  m/s**

We also observed a good agreement between the Impact++ and the theoretical model of Zhao and Faltinsen (1993), with a maximal discrepancy of results around 10%. This difference is explained by geometric non-linearity of the Zhao and Faltinsen model in opposition to the Impact++ ABAQUS linearization. ABAQUS/Explicit and FLUENT calculations confirmed this fact. As we can see in [Figure 19](#), and [Figure 20](#), the five models forecast also very near values regarding the wet surface propagation velocity and maximal peak pressure. The pressure time histories are calculated at two points P<sub>1</sub> and P<sub>2</sub>, disposed on the structure generatrix at 40 mm and 90 mm respectively from the top of the wedge. The results obtained with ABAQUS/Explicit are very close to those of fully CFD software FLUENT.

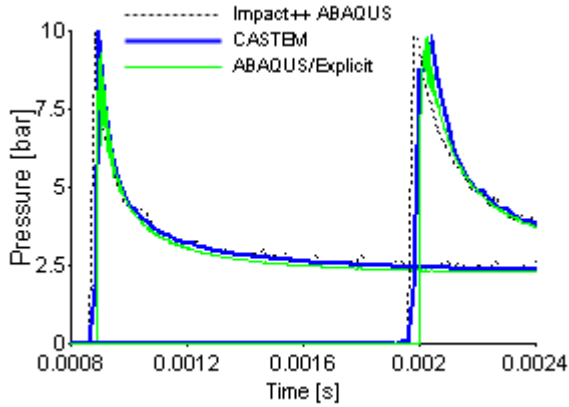


**Figure 19: Pressure vs. time at points P<sub>1</sub> and P<sub>2</sub> wedge, deadrise angle 10°, impact velocity 5 m/s**

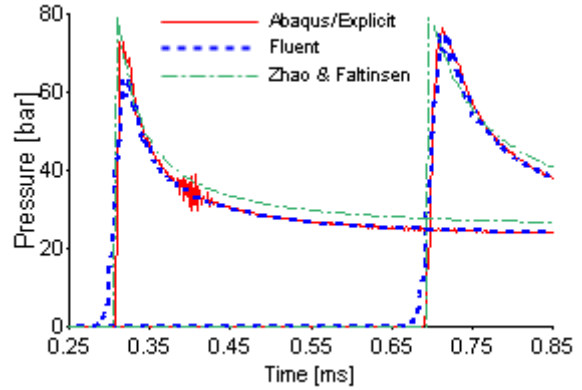


**Figure 20: Pressure vs. time at points P<sub>1</sub> and P<sub>2</sub> wedge, deadrise angle 14°, impact velocity 20 m/s**

The main result for rigid wedges is the evolution of the dimensionless expression  $f(\beta)$  expressed by the Equation 37, associated to the force per unit length  $F$  which is function of time  $t$ , deadrise angle  $\beta$ , fluid density  $\rho_f$  and entry speed  $V$ .

$$f(\beta) = \frac{F \tan^2 \beta}{\rho_f V^3 t} \quad [37]$$

According to the [Figure 21](#), the hydrodynamic forces predicted by models based on Wagner's theory, i.e. Impact++ (for small deadrise angles  $\beta$ ) and Zhao and Faltinsen analytical model, are higher compared to “non-linear” models, i.e. ABAQUS/Explicit, Fluent and Zhao and Faltinsen numerical model.

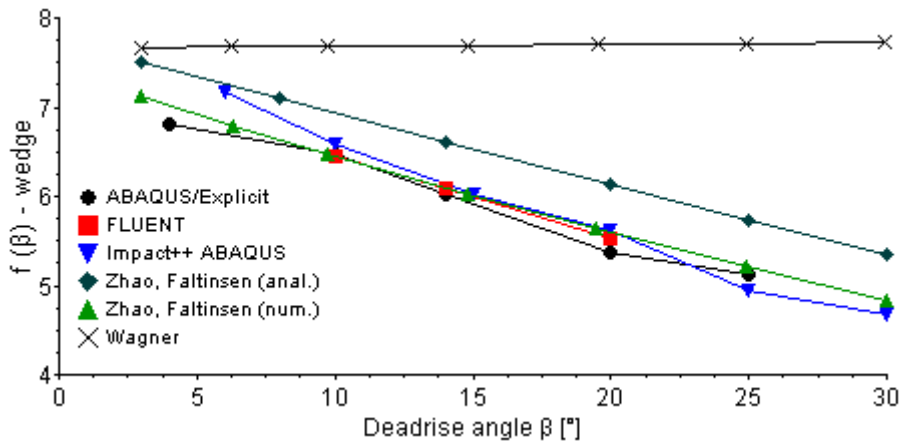


**Figure 21: Evolution of non-dimensionalized force function of deadrise angle for rigid wedges**

Regarding the cone case, we establish similar results to the wedges case concerning the total force. Thus, the hydrodynamic force predicted by Impact++ is slightly superior compared to Fluent and ABAQUS/Explicit results, [Figure 22](#). There again, the discrepancy is also around 10%. On the other hand, ABAQUS/Explicit results remain in very good agreement with those of FLUENT.

Concerning the third approach, ABAQUS/Explicit CEL provides very good results compared to Impact++ ABAQUS. In [Figure 23](#), and [Figure 24](#), the temporal evolutions of the effort obtained with the two codes are almost overcome.

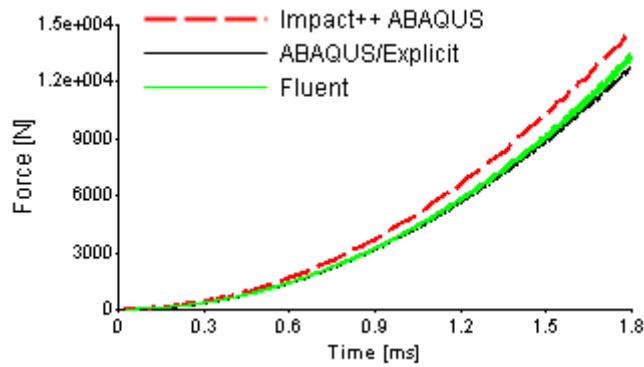


Figure 22: Force vs. time for cone of 6° deadrise angle and impact velocity of 5 m/s

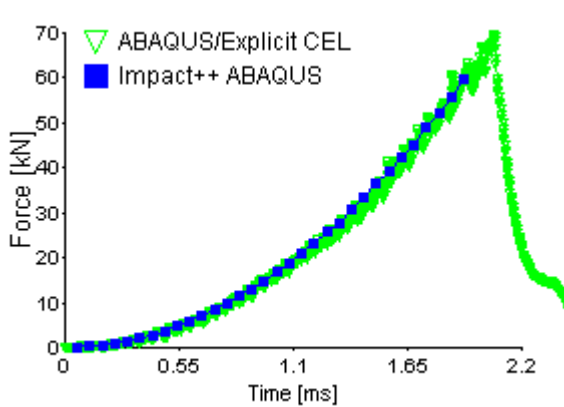


Figure 23: Force vs. time cone, deadrise angle 7°, impact velocity 8 m/s

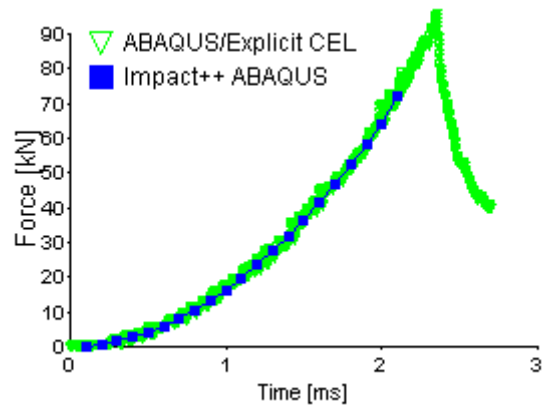


Figure 24: Force vs. time cone, deadrise angle 15°, impact velocity 15 m/s

### Comparisons between numerical and experimental results

We present in this section the experimental results obtained for the two rigid cone models. The impact velocity was set to 8 m/s for the cone having deadrise angle  $\beta = 7^\circ$ , and to 15 m/s for the cone with deadrise angle  $\beta = 15^\circ$  respectively (Figure 25, & Figure 26). The impact speed is controlled with a small error (less than 5%) which enables us to suppose that it is constant during the penetration of the structure. During the penetration of the cone into the water, the force increases up to a maximum value then, it falls brutally. This last phenomenon (loss of force) corresponds to the situation where the cone is entirely immersed and was also demonstrated numerically by Impact++ ABAQUS and ABAQUS/Explicit simulations. Moreover, according to the dimensional theory, the time evolution of the hydrodynamic force is parabolic for a rigid cone. That corresponds well to the experimental results, as presented in Figure 25, and Figure 26.

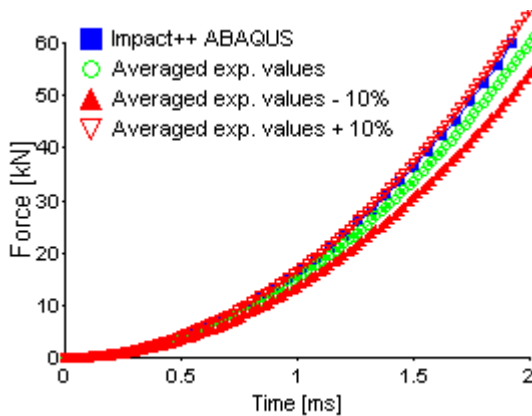


Figure 25: Force vs. time cone, deadrise angle 7°, impact velocity 8 m/s

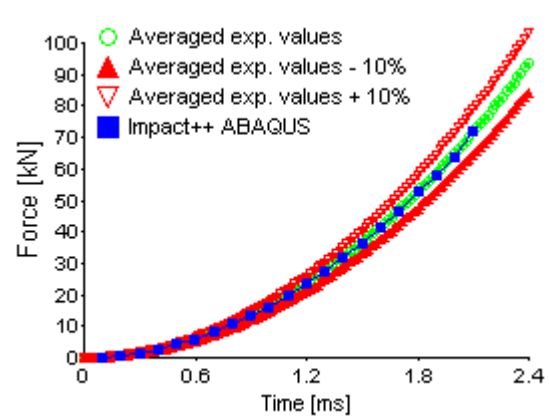


Figure 26: Force vs. time cone, deadrise angle 15°, impact velocity 15 m/s

Supp  
Mis e  
Gras  
Supp  
Mis e  
Gras  
Supp  
Supp  
Mis e  
Gras

In [Figure 25](#) and [Figure 26](#), beside the Impact++ ABAQUS results, we have represented the experimental average values obtained for the effort, as well as their upper and lower experimental limits. A statistical study reveals a high probability (90%) to obtain these experimental results. In 15° deadrise angle case, the numerical and averaged experimental results are in very good agreement. For 7° deadrise angle, the numerical results are slightly higher than the experimental values.

We have also chosen to compare the experimental results to those obtained numerically using the “non-dimensionalized” parameter related to the force. Equation 39 gives the expression of this dimensionless parameter of slamming for cones. As for wedges, the values of this parameter are theoretically constant in time for a considered deadrise angle. The simulations and the experiments confirmed well this assertion.

$$f(\beta) = \frac{F \tan^3 \beta}{\rho_f V^4 t^2} \quad [38]$$

The [Table 5](#) presents the average values of  $f(\beta)$  obtained using different FE codes and experimentally, for different deadrise angles  $\beta$ . For each entry speed, the tests generate force signals and values of  $f(\beta)$  appreciably equivalent, hence the phenomenon can be considered reproducible. The numerical and experimental studies show the non-dimensional parameter of slamming is mainly controlled by the deadrise angle of the cone. Its value is constant in time and the mass or entry speed does not influence it. [Table 5](#) shows a good results agreement between experiments, Impact++ ABAQUS, ABAQUS/Explicit and FLUENT.

**Table 5: Average values of dimensionless parameter of slamming  $f(\beta)$  for various deadrise angles for cones**

Deadrise angle	7°	15°	30°
Number of tests	11	9	
Tolerated error for experiments	10 %		-
$f(\beta)$ experimental	6.79	6.18	-
$f(\beta)$ Impact ++ ABAQUS	7.27	6.11	4.44
$f(\beta)$ ABAQUS/Explicit	7.18	6.25	4.65
$f(\beta)$ FLUENT	7.20	6.26	4.68

[Figure 27](#) shows the evolution of  $f(\beta)$  according to time. The time  $t = 0$  corresponds to the top of contact between cone and water, detected by the electrical system. In the first instants of plunging,  $f(\beta)$  is not well calculated since the measured effort  $F$  and the time  $t$  are almost zero. Afterwards,  $f(\beta)$  tends to an “asymptotic” value until the end of test (maximal impact force). Impact++ ABAQUS and experimental results for  $f(\beta)$  are found to be in good agreement, although the force  $f(\beta)$  is initially perturbed due to the undetermined form (zero force divided by zero time).

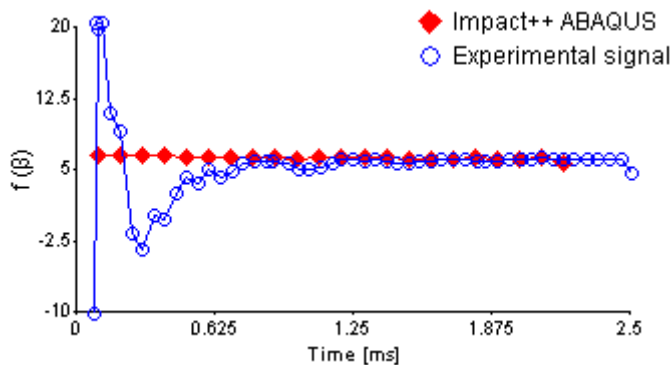


**Figure 27: Impact++ ABAQUS and experimental non-dimensionalized forces (cone,  $\beta = 15^\circ$ )**

In order to have a global comparison between experimental and numerical results for cones, we represent in the [Figure 28](#) the evolution of the non-dimensionalized expression  $f(\beta)$  expressed by the Equation 38, for different deadrise angles  $\beta$ . The experimentally hydrodynamic forces are very close to those obtained numerically. When the steady state dynamic pressure term is neglected in Equation 6 or Equation 17, Impact++ ABAQUS supplies a ‘linear’ solution higher compared to the “non-linear” solution.

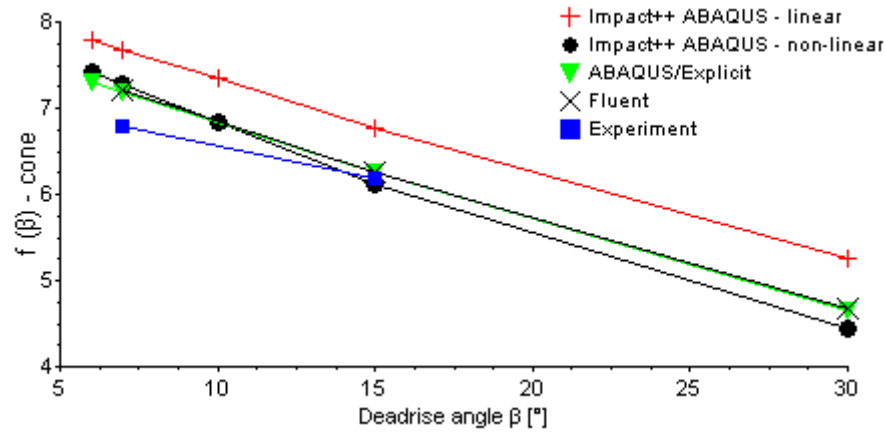


**Figure 28: Evolution of non-dimensionalized force function of deadrise angle for rigid cones**

## CONCLUSIONS

In this paper, we presented three numerical approaches able to solve two-dimensional slamming problems. A consequential experimental work completes the research work and allows us to validate these numerical tools. We have described the experimental process, including the equipment presentation, the measurement instruments and methods, as well as the choice and the dimensioning of the impacted structures. We tested two types of structure, a cone and a segment of sphere, but the results refer only to the rigid cones impacting a free water surface. The numerical and experimental efforts are in good agreement. Taking into account the asymptotic values of the non-dimensionalized parameter of slamming  $f(\beta)$ , well-predicted by the experimental results, we appreciate that the numerical results were well confirmed by these first experimental tests.

Concerning the numerical models, we described firstly the Impact++ ABAQUS approach for which the fluid problem is described by a potential formulation and an asymptotic method. The hydrodynamic pressure is corrected by analytical formula in order to take into account the formation of the jet. The pressure formulae are different between cone and wedge cases. These hybrid fluid-thermal approaches using CASTEM or ABAQUS FE codes give similar results for the propagation velocities of wetted surface and approximately 5% discrepancy for maximal pressure. The CPU time was considerably reduced using a special technique that allows to calculate velocity potentials at each time increment from a non-dimensional solution. We mention that each structure (each shape form) has its own solution. This technique must be used only for rigid structures.

ABAQUS/Explicit ALE (Arbitrary Lagrangian-Eulerian) represents the second numerical approach. It was developed initially to validate the Impact++ results, but we perceive quickly its potential in deformable and fully 3D cases. This code does not allow determining accurate pressure peaks values without very fine mesh and implicitly high CPU cost, but reliable accurate information is obtained for the resulting effort. Nevertheless, the results still rather dependent on coefficients of exponential “softened” contact law. A special attention must be accorded to this step in order to obtain a broadly contact model. Excessive grid mesh distortions were also observed during the final phase of the simulation. Globally, the ABAQUS/Explicit results are in good agreement with Impact++ ABAQUS results and particularly with those of FLUENT.

ABAQUS/Explicit CEL (Coupled Eulerian-Lagrangian) approach seems to provide very interesting and good results, compared to other numerical and experimental results, right after our first simulations. This approach proves to be a potential way to study 3D slamming notwithstanding certain limitations.

## ACKNOWLEDGMENTS

We are grateful to Steven Kerampran from ENSIETA, Brest, for supplying numerical results with the CDF code FLUENT, to University of Liege for the Post-doctoral Fellowship and the MARSTRUCT FP6-PLT-506141 EU Project. We are also thankful to DGA/MRIS for financial support in the experimental study of slamming.

## REFERENCES

KARMAN, T. von, "The impact of seaplane floats during landing", NACA Technical Notes 321, 1929

WAGNER, H., "Über Stoss-und Gleitvorgänge an der Oberfläche von Flüssigkeiten", ZAMM, Vol. 12, pp. 193-215, 1932

ZHAO, R. and O. M. FALTINSEN, "Water entry of two-dimensional bodies", Journal of Fluid Mechanics, Vol.246, pp. 593-612, 1993

BERTRAM, V., "Practical Ship Hydrodynamics", Butter-worth+Heinemann Oxford, 2002

LANGRAND, B. and E. DELETOMBE, "De la validité des comparaisons calculs/essais dans les problèmes couplés fluide/structure", 15<sup>th</sup> French Congress of Mechanics, Nancy, 2001

SCOLAN Y.M. and A. A. KOROBKIN, "Three-dimensional theory of water impact. Part 1. Inverse Wagner problem", Journal of Fluid and Mechanics, Vol. 440, pp. 293-326, 2001

DONGUY, B., 2002, "Study of the fluid interaction structure at the time of the hydrodynamic impact", Ph. D. Thesis, ECN, Nantes, France;

HIBBIT, KARLSSON and SORENSEN Inc., "ABAQUS Analysis User's Manual. Volume V: Prescribed Conditions, Constraints & Interactions", 2004

CONSTANTINESCU, A., "2D modeling of the impact of a body on water. Damage initialization", Ph.D. Thesis, Ensietia, Brest, France, 2006